

Supporting Information for

## Transitions of Two Magnetic Interaction States in Dinuclear Dy(III) Complexes via Subtle Structural Variations

Kun Zhang,<sup>[a]</sup> Dan Liu,<sup>[b]</sup> Veacheslav Vieru,<sup>[b]</sup> Lei Hou,<sup>[a]</sup> Bin Cui,<sup>[a]</sup> Fu-Sheng Guo,<sup>\*,[a]</sup> Liviu F. Chibotaru,<sup>\*,[b]</sup> and Yao-Yu Wang<sup>\*,[a]</sup>

<sup>[a]</sup> Key Laboratory of Synthetic and Natural Functional Molecule Chemistry of the Ministry of Education, Shaanxi Key Laboratory of Physico-Inorganic Chemistry, College of Chemistry & Materials Science, Northwest University, Xi'an, 710127, P.R.China.

<sup>[b]</sup> Theory of Nanomaterials Group, Department of Chemistry, KU Leuven, Celestijnenlaan 200F, 3001 Leuven, Belgium.

E-mail: [guofush@hotmail.com](mailto:guofush@hotmail.com); [wyaoyu@nwu.edu.cn](mailto:wyaoyu@nwu.edu.cn); [liviuchibotaru@chem.kuleuven.be](mailto:liviuchibotaru@chem.kuleuven.be)

### Supplementary Information Contents

Page	Title
S1	Experimental procedures and synthesis of complexes <b>1</b> and <b>2</b> .
S3	Table S1. Crystal data and structure refinement parameters for complexes <b>1</b> and <b>2</b> .
S3	Table S2. Selected bond lengths (Å) and angles (°) for complexes <b>1</b> and <b>2</b> .
S4	Figure S1. Experimental and simulated PXRD patterns for complexes <b>1</b> and <b>2</b> .
S4	Figure S2. Crystallographic packing diagrams for complexes <b>1</b> and <b>2</b> .
S5	Table S3. SHAPE analysis of the Dy(III) ion in complexes <b>1</b> and <b>2</b> . Figure S3. The mass spectrometry analysis of <b>1</b> and <b>2</b> in methanol.
S8	Figure S4. Field dependence of the magnetization, $M$ , at 2, 3 and 5 K for for complexes <b>1</b> and <b>2</b> plotted as $M$ vs. $H$ . Figure S5. Field dependence of the magnetization, $M$ , at 2, 3 and 5 K for for complexes <b>1</b> and <b>2</b> plotted as $M$ vs. $HT^{-1}$ . Figure S6. Magnetic hysteresis loops for complexes <b>1</b> and <b>2</b> at 1.8 K.
S9	Figure S7. Frequency dependence of the in-phase ( $\chi'$ ) and the out-of-phase ( $\chi''$ ) AC susceptibility component at different dc fields for complex <b>1</b> at 2 K. Table S4. Relaxation fitting parameters from Least-Squares Fitting of $\chi(f)$ between 1 and 1488 Hz data under a zero dc field of complex <b>2</b> .
S10	Table S5. Contractions of the employed basis sets in computational approximations for basis <b>1</b> and basis <b>2</b> .
S11	Table S6. Energies of the lowest Kramers doublets (KDs) ( $\text{cm}^{-1}$ ) of the Dy ion in complex <b>1</b> . Table S7. Energies of the lowest Kramers doublets (KDs) ( $\text{cm}^{-1}$ ) of the Dy ion in complex <b>2</b> . Table S8. The $g$ -tensors of the lowest Kramers doublets (KDs) ( $\text{cm}^{-1}$ ) of the Dy ion in complex <b>1</b> .
S12	Table S9. The $g$ -tensors of the lowest Kramers doublets (KDs) ( $\text{cm}^{-1}$ ) of the Dy ion in complex <b>2</b> . Table S10. Low-lying exchange levels ( $\text{cm}^{-1}$ ) for complexes <b>1</b> and <b>2</b> .

## Experimental section

### Materials

All reagents were purchased from commercial sources and were used as received. We prepared 2-(2-hydroxy-3-methoxybenzylideneamino)phenol ( $H_2L$ ) by condensation of 2-aminophenol and o-vanillin at a 1:1 molar ratio in hot ethanol according to a modified version of a previously reported procedure.<sup>S1</sup> All reactions were carried out under aerobic conditions.

[S1] H. S. Ke, L. Zhao, Y. Guo and J. K. Tang, *Inorg. Chem.* 2012, **51**, 2699–2705.

**Synthesis of complex 1**  $Dy_2(L)_2(DBM)_2(DMA)_2 \cdot 2DMA \cdot 2CH_3CN$ . We prepared a mixture of Schiff-base  $H_2L$  ligand (0.2 mmol, 48.6 mg) and triethylamine (0.4 mmol, 0.06 mL) in acetonitrile (5 mL) and stirred the solution at room temperature for 30 min. Then, solid  $Dy(NO_3)_3 \cdot 6H_2O$  (0.3 mmol, 131.6 mg) was added and further stirred for 1 h. Next, after stirring for 30 min at room temperature, DMA (5 mL) solution with dibenzoylmethane (HDBM 44.8 mg, 0.2 mmol) and triethylamine (0.2 mmol, 0.03 mL) was added to the above mixture. The resulting solution was stirred for 90 min at room temperature and filtered, and then the filtrate was allowed to stand at room temperature for 1 week. Yellow block-shaped crystals suitable for single-crystal analysis formed as a result of slow evaporation of the solvent and were collected by careful filtration; the yield was 62% based on the Dy content. We obtained infrared (IR) spectra at the following frequencies ( $cm^{-1}$ ): 3415 (m), 2929 (m), 1608 (s), 1554 (s), 1520 (s), 1454 (s), 1394 (s), 1311 (m), 1281 (m), 1221 (m), 1178 (m), 1105 (m), 1072 (m), 1018 (m), 966 (m), 818 (m), 731 (m), 687 (m), 590 (m), and 511 (m). Elemental analysis found (calc.)% for complex 1: C: 55.61 (55.52); H: 5.15 (4.98); N: 6.65 (6.60).

**Synthesis of complex 2**  $[Dy_2(L)_2(DBM)_2(DMF)_2]$ . Complex 2 was synthesized using a process similar to that used for complex 1, except that we used DMF as the axial coordination solvent ligand instead of DMA. Yellow block-shaped crystals were formed by slow evaporation of the solvent and were collected by careful filtration; the yield was 72% based on the Dy content. We obtained IR spectra at the following frequencies ( $cm^{-1}$ ): 3410 (m), 1655 (s), 1604 (s), 1554 (s), 1514 (s), 1448 (s), 1388 (s), 1311 (m), 1279 (m), 1219 (m), 1173 (m), 1101 (m), 1066 (m), 1022 (m), 964 (m), 816 (w), 742 (m), 679 (m), 607 (w), and 509 (m). Elemental analysis found (calc.)% for complex 2: C: 54.76 (54.90); H: 4.08 (4.18); N: 3.95 (4.00).

### Measurement Details

Elemental analyses (C, H, N) were performed using an Elementar Vario EL III Analyzer. The Fourier transform (FT)-IR spectra were recorded from KBr pellets in the range from 4000 to 400  $cm^{-1}$  using a Bruker Tensor 27 spectrometer. The magnetization data were recorded using a Quantum Design MPMS-XL SQUID magnetometer equipped with a 5 T magnet. Variable-temperature magnetization was measured with an external magnetic field of 500 Oe over the temperature range from 1.9 to 300 K and the frequency dependent AC susceptibility was measured with an oscillating field of 3.5 Oe. Finely ground

microcrystalline powders of complexes **1** and **2** were immobilized in an eicosane matrix inside a polycarbonate capsule. The contributions of the eicosane and the capsule were both subtracted from the data we obtained. Phase purity was checked by means of powder X-ray diffraction (PXRD) using a Bruker AXS D8 Advance diffractometer with Cu-K $\alpha$  ( $\lambda = 1.54056 \text{ \AA}$ ) radiation. The electrospray ionization mass spectrometry data were collected using a Bruker microTOF-QII mass spectrometer. The spectrometer was previously calibrated with sodium formate by switching the sheath liquid to a solution containing 5 mM sodium hydroxide in 0.2% formic acid in a water/isopropanol 1:1 v/v mixture, and we achieved a precision of ca. 1.5 ppm in the region from 500 to 5000  $m/z$ . The electrospray source was used with a drying nitrogen gas temperature of approximately +180 °C.

### X-ray Crystallography Study

Single-crystal X-ray diffraction measurements for complexes **1** and **2** were carried out on an Agilent Technologies SuperNova diffractometer with graphite monochromated MoK $\alpha$  radiation ( $\lambda = 0.71073 \text{ \AA}$ ) at 100 K. The structures were solved using the direct method (SHELXS) and refined by means of the full-matrix least-squares method (SHELXL) on  $F^2$ .<sup>S2,S3</sup> Anisotropic thermal parameters were used for the non-hydrogen atoms and isotropic parameters were used for the hydrogen atoms. Hydrogen atoms were added geometrically and refined using a riding model. Crystallographic data and refinement details are given in Supplemental Table S1. The results are available as Cambridge Crystallographic Data Centre (CCDC) records 1479827 for complex **1** and 1479828 for complex **2**.

[S2] G. M. Sheldrick, SHELXS-2014, Program for Crystal Structure Solution, University of Göttingen, 2014.

[S3] G. M. Sheldrick, *Acta Cryst. A.*, 2008, **64**, 112-122.

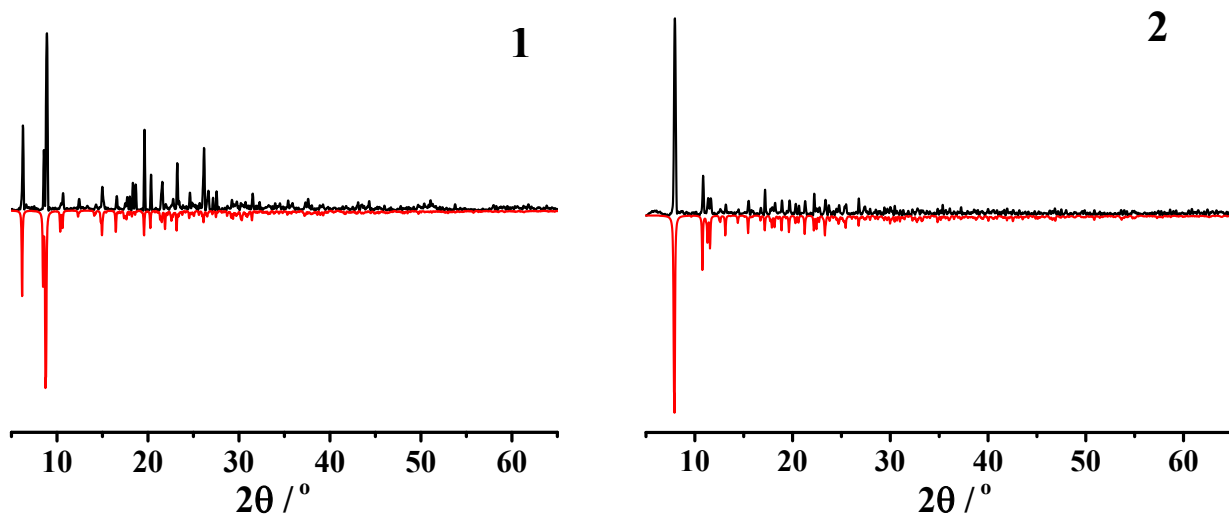
**Table S1.** Summary of the crystal data and structure refinement parameters for complexes **1** and **2**.

Complex	1	2
Formula	C <sub>78</sub> H <sub>86</sub> Dy <sub>2</sub> N <sub>8</sub> O <sub>14</sub>	C <sub>64</sub> H <sub>58</sub> Dy <sub>2</sub> N <sub>4</sub> O <sub>12</sub>
Fw	1684.55	1400.14
Temp (K)	100(1)	100(1)
Crystal system	Monoclinic	Monoclinic
Space group	<i>P2<sub>1</sub>/n</i>	<i>P2<sub>1</sub>/c</i>
<i>a</i> (Å)	17.2155(6)	11.2804(2)
<i>b</i> (Å)	12.4815(4)	15.7016(3)
<i>c</i> (Å)	17.6745(6)	15.5827(3)
$\alpha$ (°)	90	90
$\beta$ (°)	106.805(4)	95.7601(18)
$\gamma$ (°)	90	90
Volume (Å <sup>3</sup> )	3635.6(2)	2746.10(10)
<i>Z</i>	2	2
<i>D</i> <sub>calc</sub> (g cm <sup>-3</sup> )	1.539	1.693
$\mu$ (mm <sup>-1</sup> )	2.110	2.771
F (000)	1708.0	1396.0
<i>R</i> <sub>int</sub>	0.0477	0.0333
<i>R</i> <sub>sigma</sub>	0.0808	0.0542
Refl. (all)	16724	12479
Refl. (independent)	8225	6264
<i>R</i> <sub>1</sub> (all)	0.0655	0.0411
<i>wR</i> <sub>2</sub> (all)	0.1111	0.0706
<i>R</i> <sub>1</sub> (> 2 $\sigma$ )	0.0468	0.0322
<i>wR</i> <sub>2</sub> (> 2 $\sigma$ )	0.0984	0.0661
GOF.	1.040	1.036

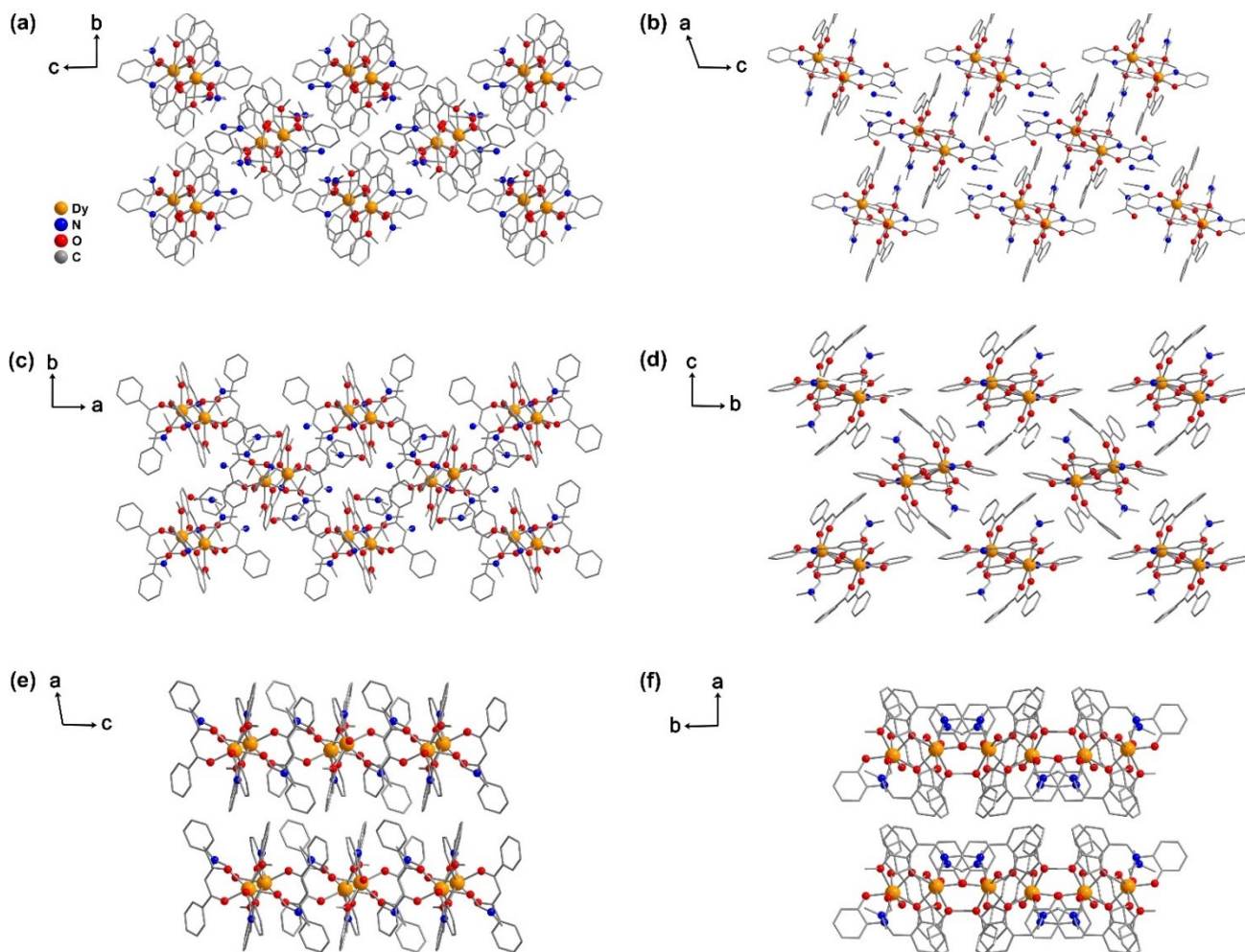
$$R_1 = \frac{\sum ||F_o| - |F_c||}{\sum |F_o|}, wR_2 = \left[ \frac{\sum w(F_o^2 - F_c^2)^2}{\sum w(F_o^2)^2} \right]^{1/2}$$
**Table S2** Selected bond lengths (Å) and angles (°) for complexes **1** and **2**.

Complex	1	2
Dy1-O1	2.348(3)	2.336(2)
Dy1-O1 <sup>a</sup>	2.368(3)	2.383(2)
Dy1-O2	2.233(3)	2.227(2)
Dy1-O3 <sup>a</sup>	2.553(4)	2.483(2)
Dy1-O4	2.305(4)	2.313(2)
Dy1-O5	2.324(3)	2.324(2)
Dy1-O6	2.370(3)	2.398(2)
Dy1-N1	2.488(4)	2.506(3)
Dy1-O1-Dy1 <sup>a</sup>	105.52(12)	106.87(9)
O1-Dy1-O1 <sup>a</sup>	74.48(12)	73.13(9)
Dy $\cdots$ Dy (Å)	3.7549(4)	3.7900(3)

Symmetry transformations used to generate equivalent atoms: for both complexes, a: 1-x, 1-y, 1-z.



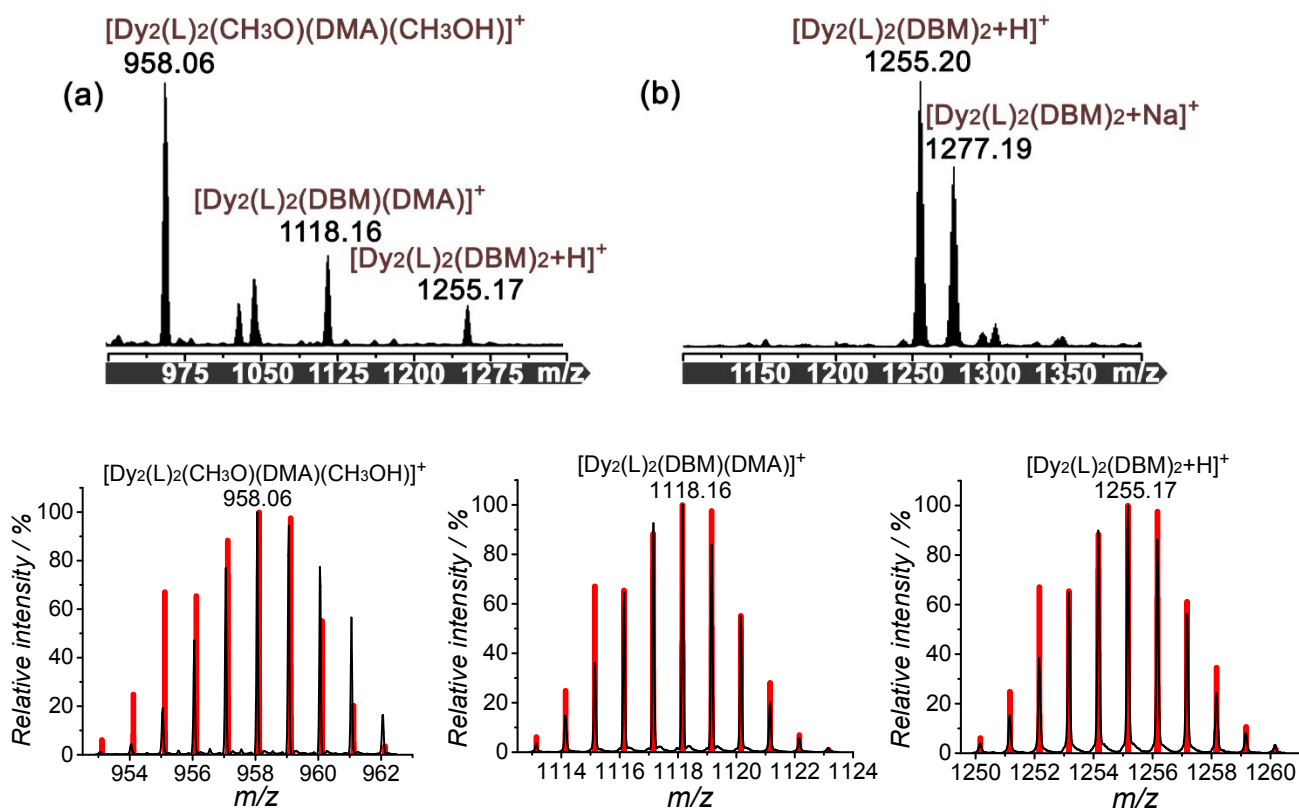
**Figure S1.** The experimental (black) and simulated (red) powder X-ray diffraction patterns for complexes **1** and **2**.



**Figure S2.** Crystallographic packing diagrams for complex **1**,  $[\text{Dy}_2(\text{L})_2(\text{DBM})_2(\text{DMA})_2] \cdot 2\text{DMA} \cdot 2\text{CH}_3\text{CN}$ , along the (a) *a*-axis, (b) *b*-axis, and (c) *c*-axis; and for complex **2**,  $[\text{Dy}_2(\text{L})_2(\text{DBM})_2(\text{DMF})_2]$ , along the (d) *a*-axis, (e) *b*-axis, and (f) *c*-axis.

**Table S3.** SHAPE analysis of the Dy(III) ion in complexes **1** and **2**.

Label	Shape	Symmetry	Distortion (1)	Distortion (2)
OP-8	Octagon	$D_{8h}$	30.344	33.133
HPY-8	Heptagonal pyramid	$C_{7v}$	24.268	23.149
HBPY-8	Hexagonal bipyramid	$D_{6h}$	15.531	14.748
CU-8	Cube	$O_h$	10.328	9.340
SAPR-8	Square antiprism	$D_{4d}$	2.116	2.841
TDD-8	Triangular dodecahedron	$D_{2d}$	1.099	0.870
JGBF-8	Johnson gyrobifastigium J26	$D_{2d}$	13.430	13.855
JETBPY-8	Johnson elongated triangular bipyramid J14	$D_{3h}$	27.882	28.439
JBTPR-8	Biaugmented trigonal prism J50	$C_{2v}$	1.379	1.795
BTPR-8	Biaugmented trigonal prism	$C_{2v}$	1.313	1.597
JSD-8	Snub diphenooid J84	$D_{2d}$	2.858	3.011
TT-8	Triakis tetrahedron	$T_d$	10.734	9.842
ETBPY-8	Elongated trigonal bipyramid	$D_{3h}$	23.941	24.728



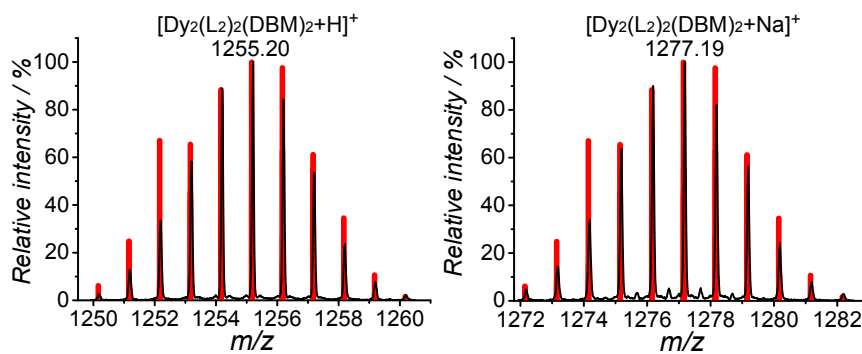


**Figure S3.** The mass spectrometry analysis of **1** (a) and **2** (b) in methanol. All calculated peaks fit the statistical treatment within experimental error. Red bars correspond to the simulated data and black lines correspond to the experimental data.

Given the structural similarity of complexes **1** and **2**, it was interesting to compare their solution behaviors. Notably, electrospray ionization mass spectrometry (ESI-MS) has been successfully applied in research on coordination chemistry to detect many different species in solution simultaneously, and thus provides at least qualitative information on complex mixtures.<sup>S4-S7</sup> Compared to d-block transition metal complexes,<sup>S8-S11</sup> there is still a lack of examples of using ESI-MS to explore the solution behaviors of structurally closely related lanthanide systems. In addition, the solution behaviors of the neutral lanthanide complexes are far from being fully understood owing to their structural flexibility, which may result in a variety of preferred ionization modes. The present  $\{\text{Dy}_2\}$  systems of complexes **1** and **2** provide good examples to learn about these behaviors.

The ESI-MS analysis of complexes **1** and **2** was performed after dissolving a few single crystals of complexes **1** and **2** in 1 mL of methanol for 10 min (Fig. S3). This solution was diluted to 10% of its original concentration by adding methanol before injection into the instrument, and the data were collected in the ESI-MS positive-ion mode. The ESI-MS analysis performed on complex **1** showed intact  $[\text{Dy}_2\text{O}_2]$  units, which exhibit a series of single-charged positive ion peaks in the range of  $m/z = 958$  to 1255. The highest-intensity peak (measured  $m/z = 958.06$ , versus calculated  $m/z = 958.11$ ) belonged to  $[\text{Dy}_2(\text{L})_2(\text{CH}_3\text{O})(\text{DMA})(\text{CH}_3\text{OH})]^+$ , as a result of the intact neutral complex **1** ( $[\text{Dy}_2(\text{L})_2(\text{DBM})_2(\text{DMA})_2] \cdot 2\text{DMA} \cdot 2\text{CH}_3\text{CN}$ ) losing all guest solvent molecules, with two coordinated  $\text{DBM}^-$  and one  $\text{DMA}$  ligand replaced by  $\text{CH}_3\text{O}^-$  and  $\text{CH}_3\text{OH}$ . The ionic peak (measured  $m/z = 1118.16$ , versus calculated  $m/z = 1118.15$ ), with a weight of 160 more than  $m/z = 958.06$ , can be assigned to  $[\text{Dy}_2(\text{L})_2(\text{DBM})(\text{DMA})]^+$ , which represents loss of one coordinated  $\text{DBM}^-$ ,  $\text{DMA}$  ligands, and all guest solvent molecules. The peak observed at measured  $m/z = 1255.17$  can be assigned to  $[\text{Dy}_2(\text{L})_2(\text{DBM})_2+\text{H}]^+$  (versus calculated  $m/z = 1255.16$ ), as a result of losing all coordinated  $\text{DMA}$  ligands and guest solvent molecules, suggesting that the parent molecule's units are stable in methanol solution. The relatively intact parent complex ions were also found to be the dominant species in the ESI-MS analysis of complex **2**. Two positive-ion species could be assigned to  $[\text{Dy}_2(\text{L})_2(\text{DBM})_2+\text{H}]^+$  at measured  $m/z = 1255.20$  (versus

calculated  $m/z = 1255.16$ ) and  $[\text{Dy}_2(\text{L}_2)_2(\text{DBM})_2+\text{Na}]^+$  at measured  $m/z = 1277.19$  (versus calculated  $m/z = 1277.15$ ).

Although the central  $[\text{Dy}_2\text{O}_2]$  core species were observed in solution for both complexes **1** and **2**, the qualitative and quantitative peaks for the cationic fragments (Fig. S3) give further evidence of different solution stability of the neutral parent entities of these structurally related complexes. Unlike the relatively straightforward spectrum of complex **2**, more complex fragment species appeared for complex **1** in solution. Surprisingly, the most dominant species of  $[\text{Dy}_2(\text{L}_2)_2(\text{DBM})_2+\text{H}]^+$  in the spectrum of complex **2** was also observed in complex **1**, but at a lower relative intensity, simultaneously accompanied by further decomposition species of  $[\text{Dy}_2(\text{L})_2(\text{DBM})(\text{DMA})]^+$  after losing a  $\text{DBM}^-$  ligand and with higher relative intensity, and  $[\text{Dy}_2(\text{L})_2(\text{CH}_3\text{O})(\text{DMA})(\text{CH}_3\text{OH})]^+$  after losing all  $\text{DBM}^-$  and becoming the dominant species in complex **1**.

Because of the relatively high pressure in the first chamber of the ESI-MS, collisions with nitrogen atoms from the bath gas occur many times. This effect tends to stabilize the ionic complexes to their ground state with respect to internal energy, and thus the more thermodynamically stable frameworks survive.<sup>S12</sup> Therefore, based on our observations of the different magnitudes of the fragment species to the integral frameworks of complexes **1** and **2** (more fragment species for complex **1**), it is reasonable to speculate that the parent framework of complex **1** is thermodynamically less stable in solution, which is consistent with the structural analysis described in main text, in which complex **1** is slightly compressed (with smaller Dy-O-Dy angle and the Dy···Dy distance than complex **2**) and may possess more steric strain than complex **2**, and is thus thermodynamically less stable.

**Note:** Ionization of a neutral analyte often occurs by cationization, with an adventitious cation such as  $\text{Na}^+$  present in the solvent that is being used. Such cations are present in solvents, and especially in polar solvents, that have been stored in glass bottles.<sup>S13</sup> In our case,  $\text{Na}^+$  ions could have been introduced during the reaction process when the reactants were kept in glass bottles, or during the process of calibration of the instrument, which was performed using sodium formate.

[S4] H. N. Miras, E. F. Wilson and L. Cronin, *Chem. Commun.*, 2009, **45**, 1297-1311.

[S5] R. Chakrabarty, P. S. Mukherjee and P. J. Stang, *Chem. Rev.*, 2011, **111**, 6810–6918.

[S6] H. I. A. Phillips, A. V. Chernikov, N. C. Fletcher, A. E. Ashcroft, J.R. Ault, M. H. Filby and A. J. Wilson, *Chem. Eur. J.* 2012, **18**, 13733–13742.

[S7] M. M. J. Smulders, I. A. Riddell, C. Browne and J. R. Nitschke, *Chem. Soc. Rev.*, 2013, **42**, 1728-1754.

[S8] Y. L. Zhou, M. H. Zeng, L. Q. Wei, B. W. Li and M. Kurmoo, *Chem. Mater.*, 2010, **22**, 4295-4303.

[S9] K. Zhang, J. Dai, Y. H. Wang, M. H. Zeng and M. Kurmoo, *Dalton Trans.*, 2013, **42**, 5439-5446.

[S10] L. Q. Wei, K. Zhang, Y. C. Feng, Y. H. Wang, M. H. Zeng and M. Kurmoo, *Inorg. Chem.*, 2011, **50**,

7274-7283.

[S11] K. Zhang, M. Kurmoo, L. Q. Wei, and M. H. Zeng, *Sci. Rep.*, 2013, **3**, 3516.

[S12] P. Kebarle and L. Tang, *Anal. Chem.*, 1993, **65**, 972-986.

[S13] W. Henderson and J. S. McIndoe, *Mass Spectrometry of Inorganic, Coordination and Organometallic Compounds: Tools - Techniques - Tips*, John Wiley & Sons, Chichester, 2005.

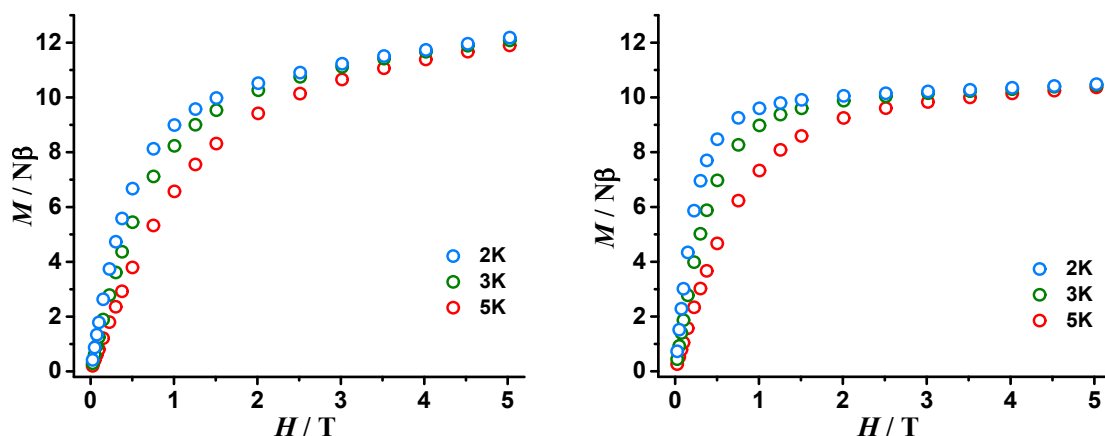


**Figure S4.** Field dependence of the magnetization,  $M$ , at 2, 3 and 5 K for complexes **1** (left) and **2** (right) plotted as  $M$  vs.  $H$ .

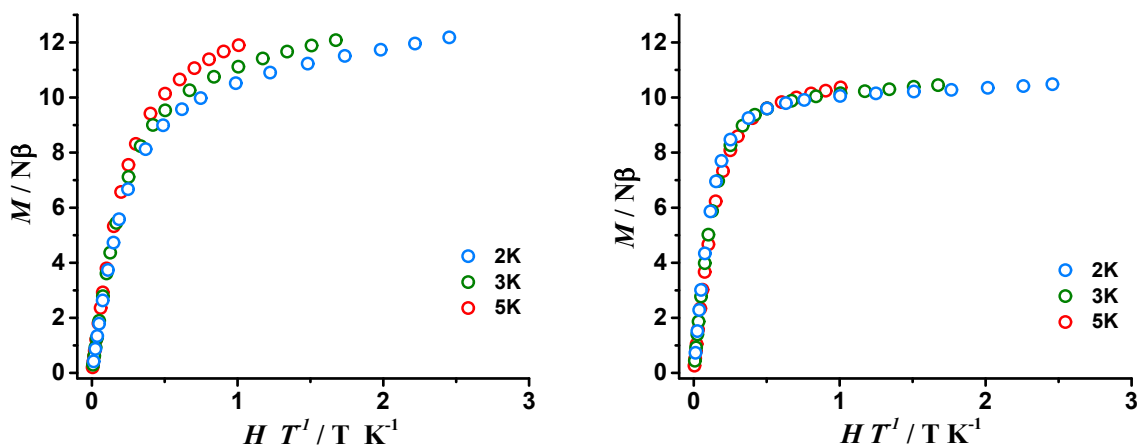


**Figure S5.** Field dependence of the magnetization,  $M$ , at 2, 3 and 5 K for for complexes **1** (left) and **2** (right) plotted as  $M$  vs.  $HT^{-1}$ .

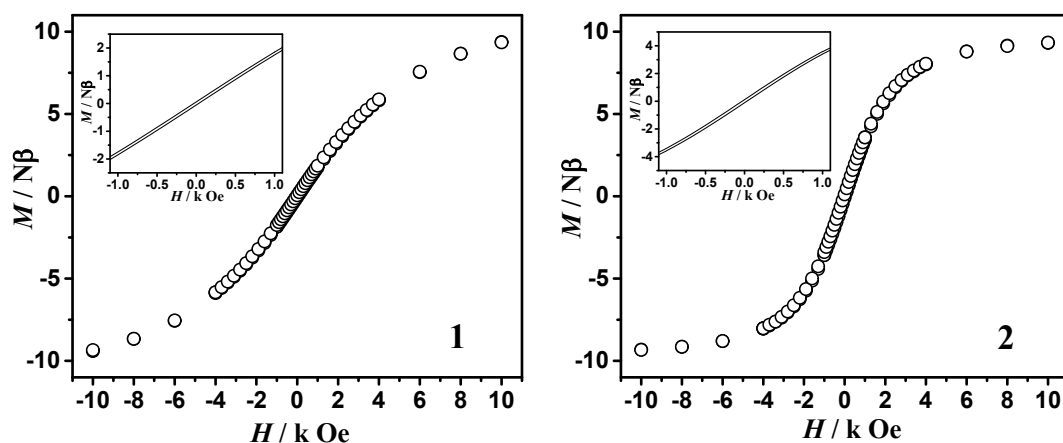


**Figure S6.** Magnetic hysteresis loops for complexes **1** and **2** at 1.8 K.

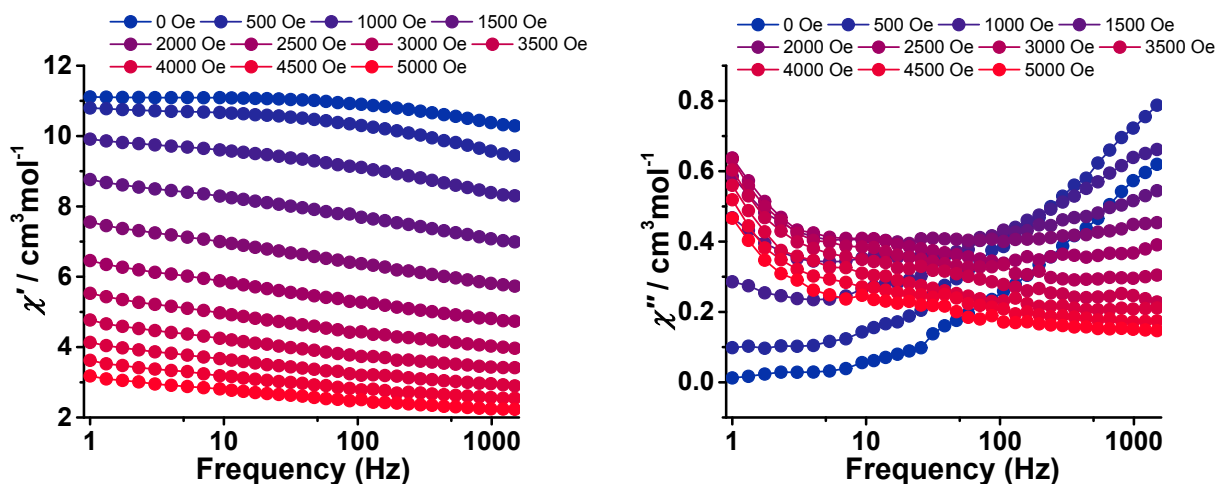


**Figure S7.** Frequency dependence of the in-phase ( $\chi'$ , left) and out-of-phase ( $\chi''$ , right) AC susceptibility component to different dc fields for complex 1 at 2 K.

**Table S4.** Relaxation fitting parameters from least-squares fitting of  $\chi(f)$  between 1 and 1488 Hz under zero dc field for complex 2.

Temperature (K)	$\chi_T$	$\chi_s$	$\alpha$	$\tau$
2.0	18.2	1.31	0.312	0.002
2.3	15.4	1.36	0.319	0.002
2.6	13.2	1.44	0.325	0.001
2.9	11.5	1.55	0.328	0.001
3.2	10.2	1.62	0.328	9.23E-4
3.5	9.13	1.55	0.340	6.73E-4
3.8	8.29	1.25	0.375	3.95E-4
3.9	7.97	0.70	0.392	2.60E-4
4.0	7.63	0.35	0.414	1.73E-4

## Computational details

All calculations were carried out with version 8.0 of the MOLCAS software (<http://www.molcas.org/>) and were of the CASSCF/RASSI/SINGLE\_ANISO type.

The Dy centers were calculated keeping the entire molecule and using the experimentally determined coordinates of the atoms. The neighboring Dy ions were replaced by lutetium (Lu).

Two basis set approximations were employed: basis **1** – small, and basis **2** – large. Table S4 shows the contractions of the employed basis sets for all elements.

**Table S5.** Contractions of the employed basis sets in computational approximations for basis **1** and basis **2**.

Basis 1	Basis 2
Dy.ANO-RCC...7s6p4d2f1g.	Dy.ANO-RCC...8s7p5d3f2g1h
Lu.ANO-RCC...7s6p4d2f.	Lu.ANO-RCC...7s6p4d2f.
N.ANO-RCC...3s2p.	N.ANO-RCC...3s2p1d.
O.ANO-RCC...3s2p.	N.ANO-RCC...3s2p.
C.ANO-RCC...3s2p.	O.ANO-RCC...3s2p1d.
H.ANO-RCC...2s.	O.ANO-RCC...3s2p.
	C.ANO-RCC...3s2p.
	H.ANO-RCC...2s.

The active space of the CASSCF method included 9 electrons in 7 orbitals (4*f* orbitals of the Dy(III) ion). All seven doublet states were mixed by spin-orbit coupling.

On the basis of the resulting spin-orbital multiplets, the SINGLE\_ANISO program computed local magnetic properties (*g*-tensors, magnetic axes, local magnetic susceptibility, etc.).

## Electronic and magnetic properties of the Dy center

**Table S6.** Energies of the lowest Kramers doublets (KDs) ( $\text{cm}^{-1}$ ) of the Dy ion in complex **1**.

Spin-orbit energies, $\text{cm}^{-1}$	
Dy_basis1	Dy_basis2
0.000	0.000
92.603	107.897
108.242	125.007
148.092	176.344
202.151	228.122
226.210	250.802
282.159	351.171
403.121	414.537

**Table S7.** Energies of the lowest Kramers doublets (KDs) ( $\text{cm}^{-1}$ ) of the Dy ion in complex **2**.

Spin-orbit energies, $\text{cm}^{-1}$	
Dy_basis1	Dy_basis2
0.000	0.000
137.610	150.760
168.057	164.255
198.488	216.079
250.133	273.294
294.550	331.412
326.062	351.774
417.040	386.754

**Table S8.** The  $g$ -tensors of the lowest Kramers doublets (KDs) ( $\text{cm}^{-1}$ ) of the Dy ion in complex **1**.

KD	Dy_basis1		Dy_basis2	
		$g$		$g$
<b>1</b>	$g_x$	0.069825		0.029288
	$g_y$	0.115297		0.046936
	$g_z$	19.296036		19.379260
<b>2</b>	$g_x$	0.055954		0.035740
	$g_y$	1.382065		0.228911
	$g_z$	16.865722		19.055694
<b>3</b>	$g_x$	0.739918		0.600123
	$g_y$	2.625285		1.319472
	$g_z$	14.067922		15.026542
<b>4</b>	$g_x$	0.326722		1.241939
	$g_y$	1.886242		3.166823
	$g_z$	9.349611		11.321499

**Table S9.** The  $g$ -tensors of the lowest Kramers doublets (KDs) ( $\text{cm}^{-1}$ ) of the Dy ion in complex **2**.

KD	Dy_basis1		Dy_basis2	
		$g$		$g$
<b>1</b>	$g_X$	0.012521		0.000311
	$g_Y$	0.015239		0.005172
	$g_Z$	19.461530		19.459286
<b>2</b>	$g_X$	0.411500		1.055671
	$g_Y$	1.387924		2.328236
	$g_Z$	15.404019		14.034543
<b>3</b>	$g_X$	1.082085		0.352787
	$g_Y$	2.909375		1.519056
	$g_Z$	15.361059		16.269782
<b>4</b>	$g_X$	9.751557		4.452663
	$g_Y$	6.147847		5.428960
	$g_Z$	2.090557		11.106680

**Table S10.** Low-lying exchange levels ( $\text{cm}^{-1}$ ) for complexes **1** and **2**.

<b>1</b>	<b>2</b>
0.000000	0.00000000
0.000038	0.00000022
0.344501	1.35957098
0.344516	1.35957121